arXiv:1610.05886v1 [hep-th] 19 Oct 2016

Quark Mass Correction to Chiral Separation Effect and Pseudoscalar Condensate

Er-dong Guo*[1,3] and Shu Lin†[2]

[1]State Key Laboratory of Theoretical Physics, Institute of Theoretical Physics, Chinese Academy of Sciences, Beijing 100190, China

[2]School of Physics and Astronomy, Sun Yat-Sen University, No 2 University Road, Zhuhai 519082, China

[3]Kavli Institute of Theoretical Physics China, Chinese Academy of Sciences, Beijing 100190, China

October 20, 2016

Abstract

We derived an analytic structure of the quark mass correction to chiral separation effect (CSE) in small mass regime. We confirmed this structure by a D3/D7 holographic model study in a finite density, finite magnetic field background. The quark mass correction to CSE can be related to correlators of pseudo-scalar condensate, quark number density and quark condensate in static limit. We found scaling relations of these correlators with spatial momentum in the small momentum regime. They characterize medium responses to electric field, inhomogeneous quark mass and chiral shift. Beyond the small momentum regime, we found existence of normalizable mode, which possibly leads to formation of spiral phase. The normalizable mode exists beyond a critical magnetic field, whose magnitude decreases with quark chemical potential.

*guoerdong@itp.ac.cn

†linshu8@mail.sysu.edu.cn

1 Introduction and Summary

The chiral magnetic effect (CME) [1, 2, 3] and chiral separation effect (CSE) [4, 5] characterize the response of vector/axial current to the axial/vector chemical potential in external magnetic field. Both effects are manifestation of axial anomaly and are of phenomenological interest in heavy ion collision experiment. In particular, CME leads to charge separation and the interplay of CME and CSE gives rise to chiral magnetic wave (CMW) [6], which leads to charge dependent flow [7]. There have been significant experimental efforts in search of CME [8, 9, 10] and CMW [11, 12], see [13, 14, 15] and references therein.

While CME and CSE share many similarities, they are known to differ in certain aspects. The chiral magnetic current is known to be independent from quark mass, temperature etc [2]. Correction may arise in dynamical cases, where axial chemical potential is not well defined and the dynamics of axial charge becomes important [16, 17]. The chiral separation current does not suffer from the issue of axial chemical potential, but it does receive correction from quark mass [4, 18, 19]. In the static case, the correction to CSE can be derived in an ad-hoc way:

$$\nabla \cdot \mathbf{j}_5 = C\tilde{\mathbf{E}} \cdot \tilde{\mathbf{B}} + 2M_q i\bar{\psi}\gamma^5\psi, \tag{1}$$

with $C = -\frac{N_c e^2 Q^2}{2\pi^2}$. In the massless limit, we can write $\tilde{E} = -\nabla\mu_q$, with μ_q being the quark chemical potential. Since $\nabla \cdot \tilde{\mathbf{B}} = 0$, we easily arrive at the celebrated CSE

$$\nabla \cdot \mathbf{j}_5 = -\nabla \cdot \left(C\mu_q\tilde{\mathbf{B}}\right) \Rightarrow \mathbf{j}_5 = -C\mu_q\tilde{\mathbf{B}}. \tag{2}$$

To obtain the mass correction to j_5, we first write the pseudoscalar operator $\sigma_5 \equiv iM_q\bar{\psi}\gamma^5\psi$ as the response to quark chemical potential: $\sigma_5(x) = \int d^4y G_{\sigma 5n}(x-y)\mu_q(y)$. The structure of the Green's function $G_{\sigma 5n}$ can be deduced from discrete symmetry: σ_5 is odd in both parity and time reversal, thus it should contain magnetic field B, which is odd in time reversal and spatial gradient ∇, which is odd in parity. Therefore, to the lowest order in gradient, we have

$$\sigma_5 = g(M_q^2, T, \mu, \tilde{B})\tilde{\mathbf{B}} \cdot \nabla\mu_q. \tag{3}$$

Following the same steps as (2), we find correction to j_5,

$$\mathbf{j}_5 = -C\mu_q\tilde{\mathbf{B}} + 2g(M_q^2, T, \mu_q, \tilde{B})\mu_q\tilde{\mathbf{B}}. \tag{4}$$

The function g is related to the Green's function as (in momentum space)

$$g = \frac{G_{\sigma 5n}}{ik\tilde{B}}. \tag{5}$$

This relation will be confirmed analytically in model study. Note that g vanishes when the quark mass M_q vanishes. We can expand it in small M_q regime:

$$g = \#\frac{M_q^2}{T^2} + o(M_q^2) \tag{6}$$

assuming $\mu_q \ll T,\ \tilde{B} \ll T^2$. The dimensionless prefactor $\#$ is to be determined by dynamics. In fact, the analytic form of g also constraints the response of σ_5 to quark mass M_q. Note that we have assumed a spatially inhomogeneous μ_q and constant M_q. Instead, we can assume an inhomogeneous M_q and constant μ_q. This should induce vev of $\sigma_5(x) = \int d^4y G_{\sigma 5\sigma}(x-y)M_q(y)$. Consistency with (3) and (6) indicates the following correction

$$\sigma_5 = 2\#\frac{M_q\mu_q}{T^2}\tilde{\mathbf{B}}\cdot\nabla M_q + o(M_q^2), \tag{7}$$

which implies $G_{\sigma 5\sigma} = 2i\#M_q k\tilde{B}\mu_q + o(M_q)$. We will provide clear numerical evidence for this correlator in model study.

The correction to j_5 is more interesting in regime of large μ_q and $\tilde{B}$. When $\tilde{B} = 0$ and μ_q large, different instabilities have been discussed in large N_c field theory with spontaneous generation of chiral density wave [20, 21], current density [22, 23, 24] and quarkyonic spiral [25, 26, 26, 27] etc. At strong magnetic field, formation of chiral magnetic spiral [28, 29, 30] is possible. Here we discuss a different type of instability characterized by pseudoscalar condensate. This instability is already identified in [31] see also [32] in low temperature confined phase. We extended the discussion and found it only exists within a window of magnetic field. Formation of this instability leads to spontaneous generation of chiral shift, first introduced in [33], which induces further correction to j_5.

The paper is organized as follows: In Sec II, we give a brief review of the holographic model and the finite density and magnetic field background; Sec III contains a study of correlators among pseudoscalar condensate, quark condensate and quark number density in small momentum regime; Sec IV extends the study of correlators in arbitrary momentum regime and discussed the instability towards formation of spiral phase. We close the paper in Sec V with some outlooks.

2 A brief review of the model

2.1 The finite density background

We use the D3/D7 model to study the effect of finite quark mass. The background consists of N_c D3 branes and N_f D7 branes. In the probe limit $N_f \ll N_c$, the background is

simply given by black hole background sourced by D3 branes, with suppressed backreaction from D7 brane. The D3/D7 model is dual to $\mathcal{N}=4$ Super Yang-Mills (SYM) fields and $\mathcal{N}=2$ hypermultiplet fields, which transform in adjoint and fundamental representations of $SU(N_c)$ gauge group respectively. By analogy with QCD, we loosely refer to the $\mathcal{N}=4$ and $\mathcal{N}=2$ fields as gluons and quarks respectively. The black hole background of D3 branes is given by [34]:

$$ds^2 = -\frac{r_0^2}{2}\frac{f^2}{H}\rho^2 dt^2 + \frac{r_0^2}{2}H\rho^2 dx^2 + \frac{d\rho^2}{\rho^2} + d\theta^2 + \sin^2\theta d\phi^2 + \cos^2\theta d\Omega_3^2. \tag{8}$$

where

$$f = 1 - \frac{1}{\rho^4}, \quad H = 1 + \frac{1}{\rho^4}. \tag{9}$$

The temperature of the gluon plasma is given by $T = \frac{r_0}{\pi}$. Note that we set AdS radius $L = 1$. It can be reinstated by dimension. We also explicitly factorize S_5 into S_3 and two additional angular coordinates θ and ϕ. There is also a nontrivial Ramond-Ramond form

$$C_4 = \left(\frac{r_0^2}{2}\rho^2 H\right)^2 dt\wedge dx_1\wedge dx_2\wedge dx_3 - \cos^4\theta d\phi\wedge d\Omega_3. \tag{10}$$

The D7 branes share the worldvolume coordinates with D3 branes. In addition, they occupy the coordinates x_4-x_7 parametrized by the S_3 coordinates. Their position in x_8-x_9 plane can be parametrized by radius $\rho\sin\theta$ and polar angle ϕ. The rotational symmetry in the x_8-x_9 plane corresponds to $U(1)_R$ symmetry in the dual field theory. The D7 branes has an additional $U(1)_B$ symmetry carried by its worldvolume gauge field. We will use the $U(1)_R$ and $U(1)_B$ symmetries as axial and vector symmetries respectively.

We are interested in the field theory state at finite temperature and finite quark chemical potential μ_q with background magnetic field $\tilde{B}$. To this end, we introduce worldvolume gauge field $A_t(\rho)$ and $\tilde{F}_{xy} = \tilde{B}$. The embedding function $\theta(\rho)$ of D7 branes in D3 background is determined by minimizing the action including a DBI term and WZ term

$$\begin{aligned} S_{D7} &= S_{DBI} + S_{WZ}, \\ S_{DBI} &= -N_f T_{D7}\int d^8\xi\sqrt{-\det\left(g_{ab} + 2\pi\alpha'\tilde{F}_{ab}\right)}, \\ S_{WZ} &= \frac{1}{2}N_f T_{D7}(2\pi\alpha')^2\int P[C_4]\wedge\tilde{F}\wedge\tilde{F}. \end{aligned} \tag{11}$$

Here T_{D7} is the D7 brane tension. g_{ab} and $\tilde{F}_{ab}$ are the induced metric and worldvolume

field strength respectively. Defining

$$B = \frac{2\pi\alpha'}{r_0^2}\tilde{B}, \quad A_t = \frac{2\pi\alpha'}{r_0}\tilde{A}_t,$$
$$\mathcal{N} = N_f T_{D7} 2\pi^2 = \frac{N_f N_c \lambda}{(2\pi)^4}, \tag{12}$$

the action simplifies to

$$S_{DBI} = -\frac{\mathcal{N}}{2\pi^2}\int d^8\xi \sqrt{-\det\left(g_{ab}+F_{ab}\right)},$$
$$S_{WZ} = \frac{1}{4\pi^2}\mathcal{N}\int P[C_4]\wedge F\wedge F. \tag{13}$$

The asymptotic behavior of θ is given by

$$\sin\theta = \frac{m}{\rho} + \frac{c}{\rho^3} + \cdots . \tag{14}$$

The coefficients are related to bare quark mass M_q and quark condensate $\langle\bar{\psi}\psi\rangle$ [34]:

$$M_q = \frac{r_0 m}{2\pi\alpha'}, \quad \langle\bar{\psi}\psi\rangle = -2\pi\alpha'\mathcal{N}r_0^3 c. \tag{15}$$

Similarly, the asymptotic behavior of A_t determines dimensionless quark chemical potential μ and density n:

$$A_t = \mu - \frac{n}{\rho^2} + \cdots , \tag{16}$$

with physical quark chemical potential and number density given by $\mu_q = \frac{r_0\mu}{2\pi\alpha'}$ and $n_q = 4\pi\alpha'\mathcal{N}r_0^3 n$.

The phase diagram of the system has been obtained in [35, 36, 37, 38, 39]. There are two possible embeddings with D7 branes crossing/not crossing the black hole horizons, corresponding to meson melting/mesonic phase respectively [40]. We will focus on meson melting phase for studying CSE in quark gluon plasma (QGP).

2.2 CSE at finite quark mass

We consider the fluctuation of embedding function ϕ in the above background. The part of quadratic action containing ϕ can be written in the following form

$$S = \mathcal{N}\int d^5x\left(-\frac{1}{2}\sqrt{-G}G^{MN}\partial_M\phi\partial_N\phi\right) - \mathcal{N}\kappa\int d^5x\Omega\epsilon^{MNPQR}F_{MN}F_{PQ}\partial_R\phi, \tag{17}$$

with $M = t, x_1, x_2, x_3, \rho$. For the evaluation of CSE, we need

$$\Omega = \cos^4\theta, \quad \kappa = \frac{1}{8}. \tag{18}$$

We do not need explicit form of G^{MN} for now. The axial current is defined by [41]

$$J_R^\mu = \int d\rho \frac{\delta \mathcal{L}}{\delta \partial_\mu \phi}. \tag{19}$$

Using EOM of ϕ, we obtain the following non-conservation equation of axial current

$$\partial_\mu J_R^\mu + \frac{\delta \mathcal{L}}{\delta \partial_\rho \phi}|_{\rho=\rho_h}^{\infty} = 0. \tag{20}$$

We will identify J_R as axial current. The non-conservation of J_R follows from two boundary terms in the integration. The boundary term at $\rho = \infty$ is related to axial anomaly:

$$\begin{aligned} O_\phi &\equiv -\frac{\delta \mathcal{L}}{\delta \partial_\rho \phi}|_{\rho=\infty} \\ &= \mathcal{N} r_0^4 \sqrt{-G} G^{M\rho} \partial_M \phi|_{\rho=\infty} + \kappa \mathcal{N} r_0^4 \Omega \epsilon^{MNPQ} F_{MN} F_{PQ}|_{\rho=\infty} \\ &= O_\eta + \mathcal{N} r_0^4 E \cdot B. \end{aligned} \tag{21}$$

Note that the factor r_0^4 follows from dimension of $\mathcal{L}$. In doing this, we have chosen r_0 to set unit and work with dimensionless coordinates t, x_1, x_2, $_3$, i.e. $\partial_\mu \to r_0 \partial_\mu$. Combining with (12), we obtain $E = \frac{2\pi\alpha'}{r_0^2}\tilde{E}$ and thus $\mathcal{N} E B r_0^4 = \frac{N_f N_c}{(2\pi)^2}\tilde{E}\tilde{B}$ corresponding to the anomaly term. Therefore the term O_η corresponds to the mass term $iM_q\bar{\psi}\gamma^5\psi$[1]. The other boundary term at horizon $\rho = \rho_h$ is an artifact of the model. Its presence is tied to our modeling of axial symmetry: since we make use of $U(1)_R$ symmetry for axial symmetry, the gluon plasma is also charged under axial symmetry. The horizon term represents axial charge exchange between the quarks (fundamental matter) and gluons (adjoint matter). The term is indeed non-vanishing in known examples [41, 42]. However, we will study CSE and correlation functions in static limit. We claim the above artifact is absent in those quantities because charge exchange is not possible in static case. This can be checked explicitly.

Now we proceed to evaluate CSE, which is the axial current J_R^3. Note that $\phi = 0$ in the background, we obtain

$$J_R^3 = \mathcal{N} r_0^3 \int_{\rho_h}^{\infty} d\rho \cos^4\theta A_t' B. \tag{22}$$

We stress that had we assumed $\phi = 0$ at the beginning, we would have obtained a vanishing CSE current. The case $m = 0$ is trivial. In this case, the embedding function is given by $\theta = 0$. J_R^3 can be evaluated exactly

$$J_R^3 = \mathcal{N} r_0^3 \int_{\rho_h}^{\infty} A_t' B = \mathcal{N} r_0^3 \mu B = \frac{N_f N_c}{(2\pi)^2}\mu_q \tilde{B}. \tag{23}$$

[1]Note that the normalization of J_R is half of J_5 in field theory.

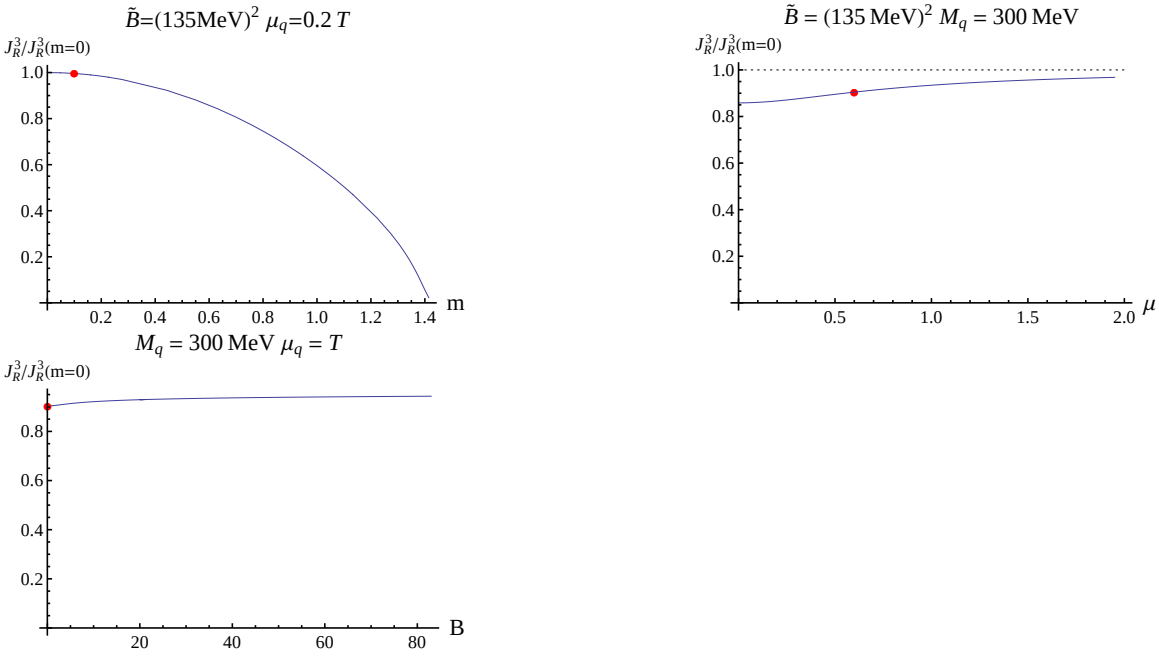

Figure 1: normalized J_R^3 as a function of m, μ and B. The temperature of QGP is set to $T = 300$MeV. To guide eyes, we mark phenomenological relevant parameters (strange quark mass $M_q = 100$MeV, $\tilde{B} = m_\pi^2$, $\mu_q = 0.5T$) with red dots in corresponding panels. In the upper right and lower panels we use $M_q = 300$MeV to magnify the dependence on $\mu(\mu_q)$ and $B(\tilde{B})$. We use $\alpha_s = 0.3$ in determination of λ. For strange quark mass $M_q = 100$MeV, the μ and B dependence is barely visible.

This is the standard CSE fixed entirely by anomaly upon restoring units in the last step. Correction to standard CSE exists for $m \neq 0$. In this case, the embedding function θ and gauge potential A_t are only known numerically. The corresponding J_R^3 can be obtained by numerical integration. We obtain its dependence on m, μ and B in Figure 1. To convert to physical unit, we use

$$r_0 = \pi T, \quad \alpha' = \frac{1}{\sqrt{\lambda}} \tag{24}$$

with phenomenologically relevant coupling and temperature. We observe that quark mass tends to suppress CSE as expected. Chemical potential and magnetic field both tends to enhance CSE. The qualitative dependence can be understood from (4). The leading term $-C\mu_q\tilde{B}$ gives the baseline 1, while the correction is

$$\Delta J_R = \#\frac{M_q^2}{T^2}\mu_q\tilde{B}. \tag{25}$$

The $m(M_q)$ dependence is quadratic, while the μ_q and $\tilde{B}$ dependence is absent at this order.

Assuming higher order terms in M_q can be ignored, the dependence in Fig.1 implies the magnitude of the prefactor # drops with growing μ_q and $\tilde{B}$. Note that the prefactor is negative, a suppressed magnitude leads to enhancement of CSE.

3 Correlators

In this section, we wish to study the correlator among scalar condensate $\sigma \equiv \bar{\psi}\psi$, pseudoscalar condensate $\sigma_5 \equiv iM_q\bar{\psi}\gamma^5\psi$ and quark number density $n_q \equiv \bar{\psi}\gamma^0\psi$. We study the Euclidean correlators at vanishing frequency (in static case when axial charge exchange is absent) and finite momentum.

$$G_{\mu\nu}(k) = \int d^4(x-y)e^{i\vec{k}\vec{x}}\langle O_\mu(x)O_\nu(y)\rangle, \tag{26}$$

with $\mu, \nu = \sigma,\ n,\ \sigma_5$. To this end, we introduce the following fluctuations to the background:

$$\theta(z,\rho) = \theta(\rho) + \delta\theta(z,\rho), \quad A_t(z,\rho) = A_t(\rho) + a_t(z,\rho), \quad \phi = \phi(z,\rho). \tag{27}$$

The open string metric up to quadratic order in fluctuation is given by

$$h_{ab} = h^{(0)}_{ab} + h^{(1)}_{ab} + h^{(2)}_{ab} + \cdots, \tag{28}$$

with

$$\begin{aligned}
h^{(0)}_{ab} &= \begin{pmatrix} g_{tt} & & -r_0A'_t \\ & g_{xx} & \\ r_0A'_t & & g_{\rho\rho}+\theta'^2 \end{pmatrix} \bigoplus \begin{pmatrix} g_{xx} & r_0^2B \\ -r_0^2B & g_{xx} \end{pmatrix} \bigoplus g_{SS}\Big(g_{\Omega 3}\Big), \\
h^{(1)}_{ab} &= \begin{pmatrix} & -r_0^2\dot{a}_t & -r_0a'_t \\ r_0^2\dot{a}_t & & r_0\delta\dot{\theta}\theta' \\ r_0a'_t & r_0\delta\dot{\theta}\theta' & 2\theta'\delta\theta' \end{pmatrix} \bigoplus \Big(0\Big) \bigoplus g^{(1)}_{SS}\Big(g_{\Omega 3}\Big), \\
h^{(2)}_{ab} &= \begin{pmatrix} r_0^2\left(\delta\dot{\theta}^2 + g_{\phi\phi}\dot{\phi}^2\right) & r_0\left(\delta\dot{\theta}\delta\theta' + g_{\phi\phi}\dot{\phi}\phi'\right) \\ r_0\left(\delta\dot{\theta}\delta\theta' + g_{\phi\phi}\dot{\phi}\phi'\right) & \delta\theta'^2 + g_{\phi\phi}\phi'^2 \end{pmatrix} \bigoplus \Big(0\Big) \bigoplus g^{(2)}_{SS}\Big(g_{\Omega 3}\Big).
\end{aligned} \tag{29}$$

Here we use the following coordinates as D7 brane worldvolume coordinates: t, z, ρ, x, y and Ω, with Ω denoting collectively three angular coordinates on S_3. They are ordered as they appear in the open string metric. It is straight forward but tedious task to work out

the quadratic action of the DBI and WZ terms

$$
\begin{aligned}
S_{\rm DBI} = &-\frac{\mathcal{N}}{2\pi^2}\int d^8\xi\sqrt{-h}\Big[\frac{r_0^2}{2}\left(\delta\dot\theta^2+g_{\phi\phi}\dot\phi^2\right)g^{xx}+\frac{1}{2}\left(\delta\theta'^2+g_{\phi\phi}\phi'^2\right)h^{\rho\rho}+\frac{3}{2}\delta g^{(2)}_{SS}g^{SS}\\
&+\frac{1}{2}r_0^4\dot a_t^2h^{tt}g^{xx}+\frac{1}{2}r_0^2a_t'^2h^{tt}h^{\rho\rho}-\frac{1}{2}r_0^2\left(\delta\dot\theta\theta'\right)^2g^{xx}h^{\rho\rho}-r_0^3\dot a_t\delta\dot\theta\theta'h^{t\rho}g^{xx}\\
&-r_0a_t'\theta'\delta\theta'h^{t\rho}h^{\rho\rho}-\frac{1}{2}\left(\delta\theta'\theta'\right)^2h^{\rho\rho 2}\\
&\frac{3}{8}\delta g^{(1)2}_{SS}\left(g^{SS}\right)^2+\frac{3}{2}\delta g^{(1)}_{SS}g^{SS}r_0a_t'h^{t\rho}+\frac{3}{2}\delta g^{(1)}_{SS}g^{SS}\theta'\delta\theta'h^{\rho\rho}\Big],\\
S_{\rm WZ} = &\frac{\mathcal{N}}{2\pi^2}r_0^4\int d^8\xi\Big[\cos^4\theta B\left(\dot a_t\phi'-a_t'\dot\phi\right)+4\cos^3\theta\sin\theta\delta\theta BA_t'\dot\phi\Big].
\end{aligned}
\tag{30}
$$

Here

$$
\begin{aligned}
&g_{SS}=\cos^2\theta,\ \ \delta g^{(1)}_{SS}=-\sin 2\theta\delta\theta,\ \ \delta g^{(2)}_{SS}=-\cos 2\theta\delta\theta^2,\\
&h^{tt}=\frac{g_{\rho\rho}+\theta'^2}{g_{tt}\left(g_{\rho\rho}+\theta'^2\right)+r_0^2A_t'^2},\ \ h^{\rho\rho}=\frac{g_{tt}}{g_{tt}\left(g_{\rho\rho}+\theta'^2\right)+r_0^2A_t'^2},\ \ h^{t\rho}=\frac{-r_0A_t'}{g_{tt}\left(g_{\rho\rho}+\theta'^2\right)+r_0^2A_t'^2},\\
&\int d^8\xi\sqrt{-h}=2\pi^2\int d^5x\sqrt{-\left(g_{tt}\left(g_{\rho\rho}+\theta'^2\right)+r_0^2A_t'^2\right)\left(g_{xx}^2+r_0^4B^2\right)g_{xx}g_{SS}^3}.
\end{aligned}
\tag{31}
$$

We use dot and prime for derivatives with respect to z and ρ respectively. Note that we work with dimensionless z, i.e. $\partial_z \to r_0\partial_z$. This amounts to setting the scale of spatial momentum by temperature. The rescaling makes the r_0 dependence of $S_{\rm DBI}$ and $S_{\rm WZ}$ appears as an overall r_0^4 factor, thus r_0 drops out completely from the EOM. The EOM following from (30) are given by

$$
\begin{aligned}
&\Big[2\sqrt{-h}\left(3\tan^2\theta-\frac{3}{2}\right)\delta\theta-3\sqrt{-h}h^{t\rho}\tan\theta a_t'+3\left(\sqrt{-h}h^{\rho\rho}\tan\theta\theta'\right)'\delta\theta+\\
&\left(\sqrt{-h}h^{t\rho}h^{\rho\rho}\theta'a_t'\right)'-\left(\sqrt{-h}h^{\rho\rho}\left(1-\theta'^2h^{\rho\rho}\right)\delta\theta'\right)'+\sqrt{-h}h^{t\rho}\theta'g^{xx}\ddot a_t\\
&-\sqrt{-h}g^{xx}\left(1-h^{\rho\rho}\theta'^2\right)\ddot\theta\Big]-4\cos^3\theta\sin\theta BA_t'\dot\phi=0,\\
&\Big[3\left(\sqrt{-h}h^{t\rho}\tan\theta\delta\theta\right)'-\left(\sqrt{-h}h^{tt}h^{\rho\rho}a_t'\right)'+\left(\sqrt{-h}h^{t\rho}h^{\rho\rho}\theta'\delta\theta'\right)'-\sqrt{-h}h^{tt}g^{xx}\ddot a_t+\sqrt{-h}h^{t\rho}g^{xx}\theta'\delta\ddot\theta\Big]\\
&-\left(\cos^4\theta\right)'B\dot\phi=0,\\
&\Big[\left(\sqrt{-h}h^{\rho\rho}\sin^2\theta\phi'\right)'+\sqrt{-h}g^{xx}\sin^2\theta\ddot\phi\Big]-\left(\cos^4\theta\right)'B\dot a_t-4\cos^3\theta\sin\theta\delta\dot\theta BA_t'=0.
\end{aligned}
\tag{32}
$$

By observation, we find the ansatz

$$
\phi(z,\rho)=\sin(kz)\phi_k(\rho),\quad a_t(z,\rho)=\cos(kz)a_t(\rho),\quad \delta\theta(z,\rho)=\cos(kz)\delta\theta(\rho),
\tag{33}
$$

solves the z-dependence of (32). To proceed, we note that a generic set of solution has the following asymptotic expansion

$$\begin{aligned}
\phi &= f_0 + \frac{f_2}{\rho^2} + \frac{f_h}{\rho^2}\ln\rho + \cdots, \\
a_t &= a_0 + \frac{a_2}{\rho^2} + \frac{a_h}{\rho^2}\ln\rho + \cdots, \\
\delta\theta &= \frac{t_1}{\rho} + \frac{t_3}{\rho^3} + \frac{t_h}{\rho^3}\ln\rho + \cdots,
\end{aligned} \tag{34}$$

where $f_h = -k^2 f_0$, $a_h = -k^2 a_0$ and $t_h = -k^2 t_1$. The leading coefficients are the sources to operators σ_5, δn and $\delta\sigma$ respectively. The subleading coefficients are related to their vevs. A holographic renormalization procedure is needed to determine the vevs. We will elaborate this procedure in appendix A. Here we only show results of correlator G_{ab}

$$\begin{aligned}
&\frac{G_{\sigma\sigma}}{(2\pi\alpha')^2\mathcal{N}r_0^2} = \frac{1}{2}S_{\sigma\sigma}, \quad \frac{G_{nn}}{(2\pi\alpha')^2\mathcal{N}r_0^2} = \frac{1}{2}S_{nn}, \quad \frac{G_{\sigma5\sigma5}}{\mathcal{N}r_0^4} = \frac{1}{2}S_{\sigma5\sigma5}, \\
&\frac{G_{\sigma n}}{(2\pi\alpha')^2\mathcal{N}r_0^2} = \frac{1}{2}S_{\sigma n}, \quad \frac{G_{n\sigma}}{(2\pi\alpha')^2\mathcal{N}r_0^2} = \frac{1}{2}S_{n\sigma} \\
&\frac{G_{\sigma\sigma5}}{(2\pi\alpha')\mathcal{N}r_0^3} = \frac{1}{2}S_{\sigma\sigma5}, \quad \frac{G_{\sigma5\sigma}}{(2\pi\alpha')\mathcal{N}r_0^3} = \frac{1}{2}S_{\sigma5\sigma}, \\
&\frac{G_{n\sigma5}}{(2\pi\alpha')\mathcal{N}r_0^3} = \frac{1}{2}S_{n\sigma5}, \quad \frac{G_{\sigma5n}}{(2\pi\alpha')\mathcal{N}r_0^3} = \frac{1}{2}S_{\sigma5n},
\end{aligned} \tag{35}$$

where we have defined individual responses S_{ab}

$$\begin{aligned}
&S_{\sigma\sigma} = \frac{\partial t_3}{\partial t_1}, \quad S_{\sigma n} = \frac{\partial t_3}{\partial a_0}, \quad S_{\sigma\sigma5} = \frac{\partial t_3}{\partial f_0}, \\
&S_{n\sigma} = -2\frac{\partial a_2}{\partial t_1}, \quad S_{nn} = -2\frac{\partial a_2}{\partial a_0}, \quad S_{n\sigma5} = -2\frac{\partial a_2}{\partial f_0}, \\
&S_{\sigma5\sigma} = m^2\frac{\partial f_2}{\partial t_1}, \quad S_{\sigma5n} = m^2\frac{\partial f_2}{\partial a_0}, \quad S_{\sigma5\sigma5} = m^2\frac{\partial f_2}{\partial f_0}.
\end{aligned} \tag{36}$$

We proceed to solve (32). Since we have three coupled differential equations, we expect to have three independent solutions. We solve (32) by numerical integration from the horizon to the boundary. The initial condition we impose at the horizon is regularity condition. In practice, we start off the horizon with the following three independent solutions:

$$\begin{aligned}
&\delta\theta^{(1)}(1+\epsilon) = 1 + O(\epsilon^2), \;\; a_t^{(1)} = O(\epsilon^2), \;\; \phi^{(1)} = O(\epsilon^2), \\
&\delta\theta^{(2)}(1+\epsilon) = O(\epsilon^2), \;\; a_t^{(2)} = \epsilon^2 + O(\epsilon^3), \;\; \phi^{(2)} = O(\epsilon^2), \\
&\delta\theta^{(3)}(1+\epsilon) = O(\epsilon^2), \;\; a_t^{(3)} = O(\epsilon^2), \;\; \phi^{(3)} = 1 + O(\epsilon^2).
\end{aligned} \tag{37}$$

These solutions give rise to the following asymptotics at the boundary

$$\begin{aligned}
\phi^{(i)} &= f_0^{(i)} + \frac{f_2^{(i)}}{\rho^2} + \frac{f_h^{(i)}}{\rho^2}\ln\rho + \cdots, \\
a_t^{(i)} &= a_0^{(i)} + \frac{a_2^{(i)}}{\rho^2} + \frac{a_h^{(i)}}{\rho^2}\ln\rho + \cdots, \\
\delta\theta^{(i)} &= \frac{t_1^{(i)}}{\rho} + \frac{t_3^{(i)}}{\rho^3} + \frac{t_h^{(i)}}{\rho^3}\ln\rho + \cdots,
\end{aligned} \tag{38}$$

with $i = 1, 2, 3$ labeling different solutions. In order to calculate individual responses S_{ab}, we need to construct proper solution for which the other two sources vanish. This can be done efficiently in the following way

$$\begin{pmatrix} S_{\sigma\sigma} & S_{n\sigma} & S_{\sigma 5\sigma} \\ S_{\sigma n} & S_{nn} & S_{\sigma 5 n} \\ S_{\sigma\sigma 5} & S_{n\sigma 5} & S_{\sigma 5\sigma 5} \end{pmatrix} = \begin{pmatrix} t_1^{(1)} & a_0^{(1)} & f_0^{(1)} \\ t_1^{(2)} & a_0^{(2)} & f_0^{(2)} \\ t_1^{(3)} & a_0^{(3)} & f_0^{(3)} \end{pmatrix}^{-1} \begin{pmatrix} t_3^{(1)} & -2a_2^{(1)} & m^2 f_2^{(1)} \\ t_3^{(2)} & -2a_2^{(2)} & m^2 f_2^{(2)} \\ t_3^{(3)} & -2a_2^{(3)} & m^2 f_2^{(3)} \end{pmatrix}. \tag{39}$$

On general ground, we expect the Euclidean correlator to be real and symmetric $G_{ab} = G_{ab}^* = G_{ba}$. Our numerical results confirm that this is indeed the case. We also find the following scaling of all individual responses at small k.

$$\begin{aligned}
&S_{\sigma\sigma},\, S_{\sigma n},\, S_{n\sigma},\, S_{nn} \sim O(k^0), \\
&S_{\sigma\sigma 5},\, S_{n\sigma 5}, S_{\sigma 5\sigma},\, S_{\sigma 5 n}, \sim O(kB), \\
&S_{\sigma 5\sigma 5} \sim O(k^2)
\end{aligned} \tag{40}$$

The first line of (40) is closely related to thermodynamics of the system. At $k = 0$, we have

$$S_{\sigma n} = \frac{\partial c(m,\,\mu)}{\partial \mu}, \quad S_{n\sigma} = \frac{\partial n(n,\,\mu)}{\partial m}. \tag{41}$$

Similarly, the diagonal responses $S_{\sigma\sigma}$ and S_{nn} are related to $\frac{\partial c}{\partial m}$ and $\frac{\partial n}{\partial \mu}$[2]. We have compared the results of individual responses at $k = 0$ and those of thermodynamics, finding expected agreement.

The second line of (40) is of more interest to us. It follows from (35) that $G_{\sigma\sigma 5},\, G_{n\sigma 5} \sim O(kB)$. This is consistent with parity (P) and time-reversal (T) symmetry of the corresponding operators: σ_5 is odd under both P and T, while σ and n are even under P and T. The external B and momentum k are odd under T and P respectively. These Euclidean correlators characterize response of the system to external parameter ϕ:

$$\sigma \sim G_{\sigma\sigma 5}\phi, \quad n \sim G_{n\sigma 5}\phi. \tag{42}$$

[2]For $S_{\sigma\sigma}$, there is correction proportional to m^2

Here we use ϕ to denote the field theory source coupled to σ_5. The scaling $O(k)$ can be understood as follows: the source ϕ enters field theory Lagrangian as $M_q\bar{\psi}e^{i\phi\gamma^5}\psi$. If we perform a chiral rotation, $\psi \to e^{-i\gamma^5\phi/2}\psi$, the relevant terms in the Lagrangian is modified as [41]

$$M_q\bar{\psi}e^{i\phi\gamma^5}\psi \to M_q\bar{\psi}\psi - \frac{\partial_\mu\phi}{2}\bar{\psi}\gamma^\mu\gamma^5\psi. \tag{43}$$

This implies that only $\partial_\mu\phi$ appears as physical parameter. In our case, ϕ only depends on z in field theory coordinates, therefore the physical parameter is $\dot{\phi}$. Interestingly, $\dot{\phi}$ can be identified as the chiral shift parameter proposed in [33, 18]. Assuming the response of σ and n to $\dot{\phi}$ is $O(1)$ at small k, we naturally explain the $O(k)$ scaling of correlators $G_{\sigma\sigma5}$, $G_{n\sigma5}$.

The third line of (40) indicates $G_{\sigma5\sigma5} \sim O(k^2)$. $G_{\sigma5\sigma5}$ is by definition the susceptibility of σ_5. The susceptibility $G_{\sigma5\sigma5}$ is parity even, thus it scales as even power of k. As we argued above, any response to ϕ has to start from $O(k)$, the most probable scaling is $O(k^2)$.

Let us take a closer look at correlators involving σ_5. We will present results primarily on these correlators at small k. In fact, we can confirm the linear scaling relation described above by perturbative calculation in k. Note that $\phi \sim O(k)$, a_t, $\delta\theta \sim O(1)$. To the lowest non-trivial order in k, we only need to solve the following equations

$$\begin{aligned}
&2\sqrt{-h}\left(3\tan^2\theta - \frac{3}{2}\right)\delta\theta - 3\sqrt{-h}h^{t\rho}\tan\theta a_t' + 3\left(\sqrt{-h}h^{\rho\rho}\tan\theta\theta'\right)'\delta\theta + \\
&\left(\sqrt{-h}h^{t\rho}h^{\rho\rho}\theta' a_t'\right)' - \left(\sqrt{-h}h^{\rho\rho}\left(1-\theta'^2h^{\rho\rho}\right)\right)' = 0, \\
&3\left(\sqrt{-h}h^{t\rho}\tan\theta\delta\theta\right)' - \left(\sqrt{-h}h^{tt}h^{\rho\rho}a_t'\right)' + \left(\sqrt{-h}h^{t\rho}h^{\rho\rho}\theta'\delta\theta'\right)' = 0, \\
&\left(\sqrt{-h}h^{\rho\rho}\sin^2\theta\phi'\right)' - \left(\cos^4\theta\right)' B\dot{a}_t - 4\cos^3\theta\sin\theta\delta\dot{\theta}BA_t' = 0.
\end{aligned} \tag{44}$$

From the first two equations of (44), we can solve for $\delta\theta$ and a_t. Plugging the solution into the third equation and integrating from the horizon to the boundary, we obtain

$$\sqrt{-h}h^{\rho\rho}\sin^2\theta\phi'|_{\rho_h}^{\infty} = \int_{\rho_h}^{\infty} d\rho\left(\cos^4\theta\right)' B\dot{a}_t + 4\cos^3\theta\sin\theta\delta\dot{\theta}BA_t' \tag{45}$$

On the left hand side (LHS), the boundary term at the horizon vanishes, the boundary term at infinity is just $-\frac{m^2 f_2}{2}$. On the right hand side (RHS), it is related to the sources t_1 and a_0. There are two independent solutions. We denote their asymptotics as

$$\begin{aligned}
\delta\theta^{(i)} &= \frac{t_1^{(i)}}{\rho} + \frac{t_3^{(i)}}{\rho^3} + \frac{t_h^{(i)}}{\rho^3}\ln\rho + \cdots, \\
a_t^{(i)} &= a_0^{(i)} + \frac{a_2^{(i)}}{\rho^2} + \frac{a_h^{(i)}}{\rho^2}\ln\rho + \cdots,
\end{aligned} \tag{46}$$

with $i = 1, 2$. Using (45), each solution give rise to vev of $\sigma_5 \sim m^2 f_2^{(i)}$. Similar to (39), we obtain the correlators as

$$\begin{pmatrix} S_{\sigma 5 \sigma} \\ S_{\sigma 5 n} \end{pmatrix} = \begin{pmatrix} t_3^{(1)} & a_0^{(1)} \\ t_3^{(2)} & a_0^{(2)} \end{pmatrix}^{-1} \begin{pmatrix} m^2 f_2^{(1)} \\ m^2 f_2^{(2)} \end{pmatrix}. \tag{47}$$

Note that at the boundary $\dot{a}_t \sim E$, $\delta\dot{\theta} \sim \delta\dot{m}$. The correlator $S_{\sigma 5 n}(G_{\sigma 5 n})$ measures the response of σ_5 to parallel E and B fields. To study the response in more detail, we define a dimensionless ratio

$$r = -\frac{\sigma_5}{\mathcal{N} E \cdot B r_0^4} \tag{48}$$

Note that we have included a minus sign in the definition of r such that r is always positive. In terms of correlators, $r = \frac{S_{\sigma 5 n}}{2ik}$. Since $S_{\sigma 5 n} \sim O(k)$, r approaches a constant in the limit $k \to 0$. We plot the m and μ-dependence of $r(k \to 0, \mu = 0)$ in Figure 2. We find r increases with m, but decreases with μ. The dependence is in qualitative agreement with our discussion before: $r \sim g \sim \#\frac{M_q^2}{T^2}$, which grows with m, and drops with μ_q from the μ_q dependence of the prefactor $\#$. Now we are in a position to confirm the claim (4) in Sec I. We begin by working in the background with $\mu = 0\,(A_t = 0)$. The corresponding correlator $G_{\sigma 5 n}$ becomes particularly simple then

$$G_{\sigma 5 n}(k \to 0) = -\left(2\pi\alpha'\right) \mathcal{N} r_0^3 \frac{\int_{\rho_h}^{\infty} d\rho \left(\cos^4\theta\right)' B \dot{a}_t}{a_t(\rho \to \infty)}. \tag{49}$$

Noting that $\frac{r_0 \mu}{2\pi\alpha'} = \mu_q$, we obtain

$$\sigma_5 = G_{\sigma 5 n}(k \to 0, \mu = 0)\mu_q = -i\mathcal{N} r_0^4 k \int_{\rho_h}^{\infty} \left(\cos^4\theta\right)' a_t B. \tag{50}$$

One the other hand, the correction to CSE can be obtained by performing an integration by part on (22)

$$\begin{aligned} J_R^3 &= \mathcal{N} r_0^3 \int d\rho \cos^4\theta A_t' B = \mathcal{N} r_0^3 \left(\cos^4\theta A_t B|_{\rho_h}^{\infty} - \int_{\rho_h}^{\infty} \left(\cos^4\theta\right)' A_t B \right) \\ &= \mathcal{N} r_0^3 \left(\mu B - \int_{\rho_h}^{\infty} \left(\cos^4\theta\right)' A_t B \right). \end{aligned} \tag{51}$$

The first term of (51) corresponds to the standard CSE, while the second term comes from mass correction, which is precisely (50). In this case, $r(k \to 0)$ takes the form

$$r(k \to 0) = \frac{\int_{\rho_h}^{\infty} d\rho \left(\cos^4\theta\right)' a_t}{a_t(\rho \to \infty)}. \tag{52}$$

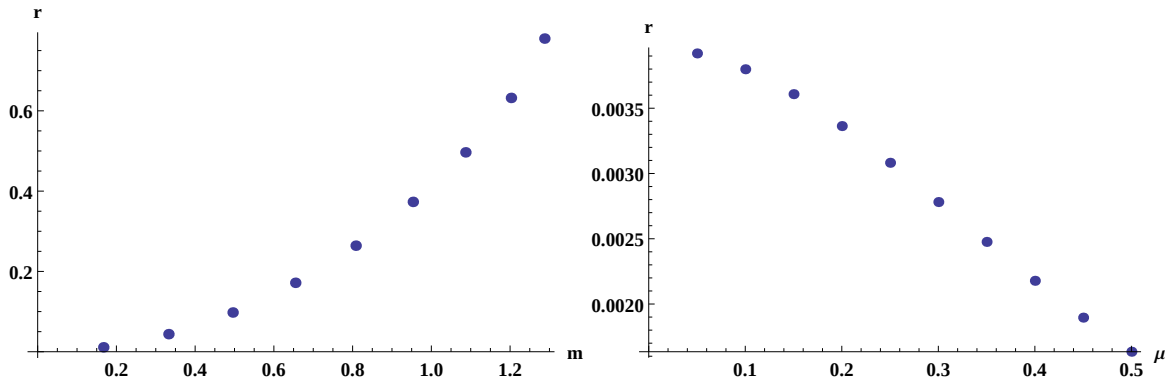

Figure 2: r defined in (48) as a function of m at $\mu = 0$ (left). Note that m is related to physical quark mass M_q by $m = \frac{2}{\sqrt{\lambda}}\frac{M_q}{T}$. The right plot shows r as a function of μ at $m = 0.1$. The ratio r increases with m, but decreases with μ.

It is instructive to analyze the coupling dependence of r: we first note that in the case $\mu = 0$, the coupling enters only through $m = \frac{2}{\sqrt{\lambda}}\frac{M_q}{T}$. On the other hand, we have argued in the introduction that $r \sim g \sim \#\frac{M_q^2}{T^2}$, which suggests the following dependence $r \sim \frac{1}{\lambda}\frac{M_q^2}{T^2}$. This seems to imply that stronger interaction leads to weaker response of σ_5 to external electromagnetic fields. This interpretation is misleading for the following reason: in D3/D7 model, the electromagnetic coupling to quark is the same as strong coupling, thus $\mathcal{N}EB \sim O(\lambda)$, so the actual response of σ_5 is $O(\lambda^0)$. It is also interesting to compare r with the same quantity studied in [43], which is defined in the regime $\omega \to 0$, $k = 0$. In fact, we can show analytically that they do not agree. For monotonic a_t, we have

$$r(k \to 0,\, \omega = 0) = \frac{\int_{\rho_h}^{\infty} d\rho \left(\cos^4\theta\right)' B a_t}{a_t(\rho \to \infty)} < \int_{\rho_h}^{\infty} d\rho \left(\cos^4\theta\right)' B = \left(1 - \cos^4\theta_h\right) B$$
$$= r(\omega \to 0,\, k = 0). \qquad (53)$$

This reveals noncommutativity of the limits $\omega \to 0$, $k \to 0$ and $k \to 0$, $\omega \to 0$ in the response of σ_5. The correlator $G_{\sigma 5 n}$ tells us more than the response of σ_5. Note that we have $G_{\sigma 5 n} = G_{n \sigma 5}$ by symmetry. $G_{n\sigma 5}$ characterizes the response of n to chiral shift $\dot{\phi}$. The result of r indicates that chiral shift can also induce correction to n in the presence of B, with the correction increases with m, but decreases with μ.

Now we turn to $S_{\sigma 5 \sigma}$. This correlator measures the response of σ_5 to spatially varying quark mass δm. We plot the m-dependence and μ-dependence of $S_{\sigma 5 \sigma}$ in Figure 3. Indeed, we can see in Fig. 3 that $G_{\sigma 5 \sigma}$ vanishes approximately linearly in μ and m, which is clear evidence for (7). By symmetry $S_{\sigma 5 \sigma} = S_{\sigma \sigma 5}$, we also obtain that chiral shift $\dot{\phi}$ can induce

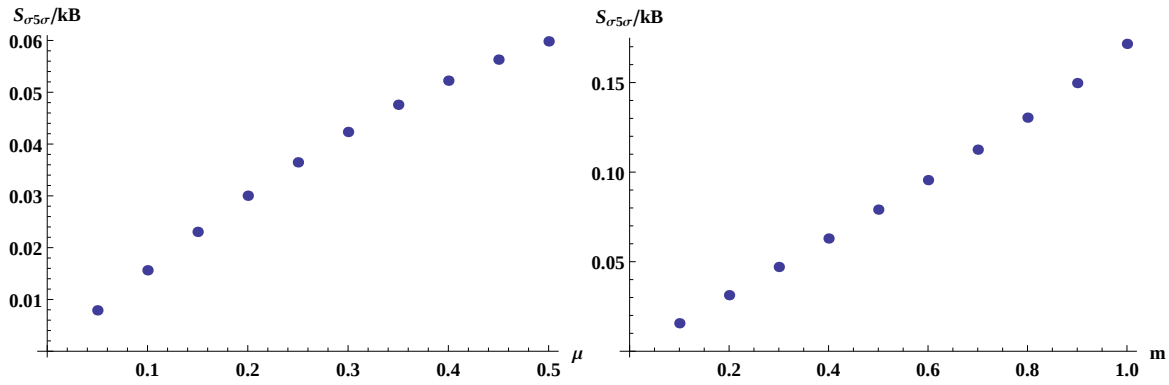

Figure 3: $\lim_{k\to 0}\frac{S_{\sigma 5\sigma}}{Bk}$ as a function of μ at $m = 0.1$ (left) and the same quantity as a function of m at $\mu = 0.1$ (right). The response of σ_5 to spatially varying mass increases with both μ and m.

correction to σ. The correction increases with both μ and m.

Finally we plot the m and μ dependence of $S_{\sigma 5\sigma 5}$ in Figure 4. The scaling $S_{\sigma 5\sigma 5} \sim O(k^2)$ allows for the following parametrization of s_5

$$\nabla \cdot \mathbf{j}_5 = 2s_5 = h(m^2, \mu, B)\nabla^2\phi. \tag{54}$$

From (54), we easily obtain an induced j_5 in the presence of chiral shift $\dot{\phi}$:

$$\mathbf{j}_5 = h(m^2, \mu, B)\nabla\phi. \tag{55}$$

A similar current from spatial gradient of axion is also discussed in [44]. As we discussed before, $\nabla\phi$ is just the chiral shift parameter, which couples to the axial current in the Lagrangian. The function h can be viewed as an effective susceptibility. Fig.4 suggests the following dependence $\frac{h}{N} = am^2 + bm^4$. Converting to physical parameters, we have $h = \#M_q^2 + O(M_q^2)$, with $\# \sim O(\lambda^0)$.

4 Normalizable mode

Now we extend our study to correlators in regime of arbitrary k. Instead of calculating all components of correlators, we look for normalizable modes. The existence of normalizable mode means that it costs no energy to support such a mode. It usually corresponds to spontaneous generation of spiral phase with the spatial period set by the momentum of the normalizable mode. The normalizable mode corresponds to the point where the determinant

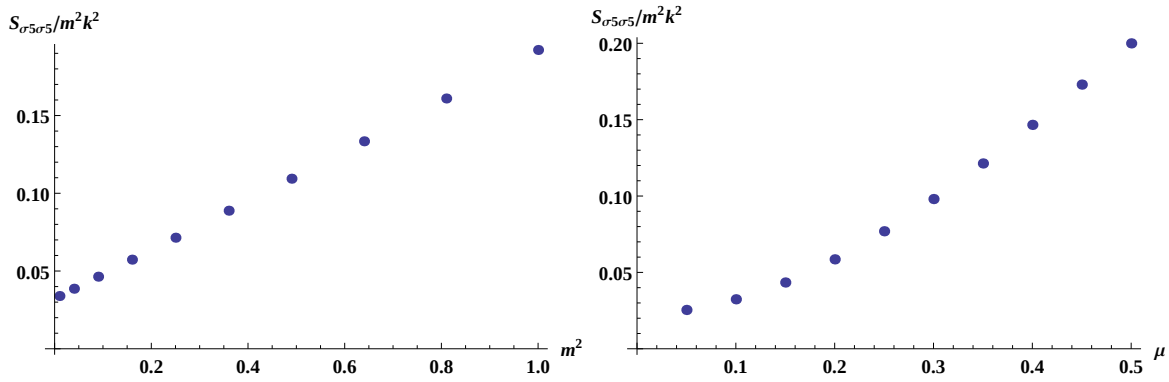

Figure 4: $\lim_{k\to 0}\frac{S_{\sigma 5\sigma 5}}{m^2k^2}$ as a function of m at $\mu = 0.1$ (left) and the same quantity as a function of μ at $m = 0.1$ (right). The left plot is suggestive of the expansion $\lim_{k\to 0}\frac{S_{\sigma 5\sigma 5}}{m^2k^2} = a + bm^2 + o(m^2)$. The right plot shows the response of σ_5 to ϕ increases with μ.

vanishes:

$$\begin{vmatrix} t_1^{(1)} & a_0^{(1)} & f_0^{(1)} \\ t_1^{(2)} & a_0^{(2)} & f_0^{(2)} \\ t_1^{(3)} & a_0^{(3)} & f_0^{(3)} \end{vmatrix} = 0 \tag{56}$$

We show the momentum k of the mode as a function of B in Figure 5. We find that one normalizable mode exists for medium with general nonvanishing μ beyond certain critical magnetic field B_c. In particular, the normalizable mode we find is numerically consistent with one of the quasi-normal mode in [31]. The normalizable mode appears at finite B_c with finite k. As B increases, the corresponding mode momentum k drops. The mode extends to the region of large B, where the state possibly becomes metastable [39]. We do not keep the corresponding mode in Fig. 5. Turning to the μ dependence, we see that as μ is lowered, B_c grows. This is qualitatively in agreement with the chiral soliton solution found in [32] in confined phase. We also show the momentum as a function of m in Fig. 5. The momentum decreases mildly with m.

To have an idea on the magnitude of magnetic field, we convert B_c for the case $\mu = 3$ to physical unit. For gluon plasma at temperature $T = 300$MeV and coupling $\alpha_s = 0.3$. This correspond to $\tilde{B}_c = (389\text{MeV})^2$ for $\mu_q = 504$MeV.

5 Outlook

We close this paper by discussing several open questions that we may address based on the results of this paper. Firstly, how does quark mass affect the dynamics of axial and

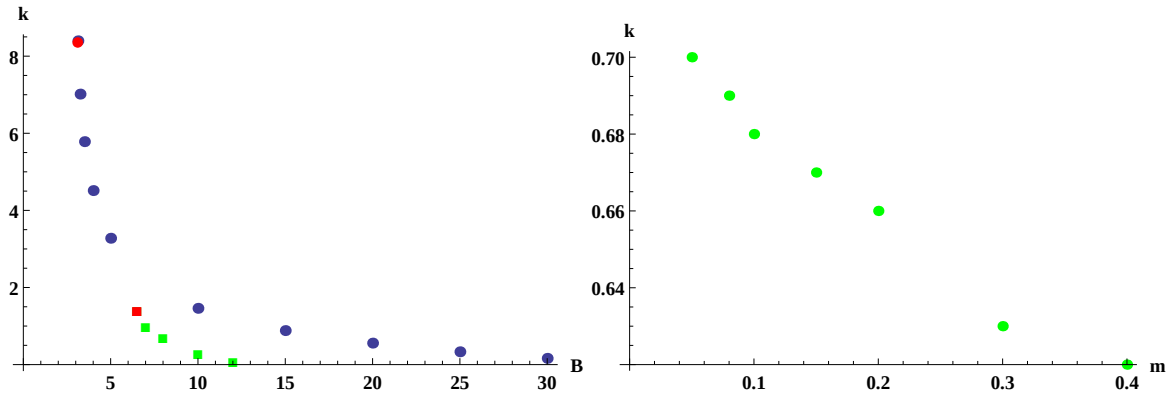

Figure 5: Momentum of normalizable mode as a function of B (left). The blue dots and green squares correspond to the cases with $\mu = 3$ and $\mu = 1$ respectively. The momentum drops as B increases. There is a critical B_c marked by red dots (squares) for each case. The normalizable mode starts to appear with finite k beyond B_c, indicating a first order transition. At larger B, the state possibly become metastable. Momentum of normalizable mode as a function of m (right). The momentum shows a mild decrease with m.

vector charge. As we have seen the pseudoscalar condensate responses to gradient of quark chemical potential etc. This brings in an additional coupling between axial and vector charges. Consequently, it should also modify the dispersion of CMW. For strange quark mass, we expect from the Fig. 1 that the modification in phenomenology is modest. Since our study focuses on Euclidean correlators, the same quantities can be reliably studied on the lattice, which will provide quantitative answers for quark mass effect in real world QCD.

Secondly, the normalizable mode we found at sufficient large B and μ suggests possible formation of spiral phase. To find the true ground state, we need to go beyond the linear analysis. We expect that the true ground state is characterized by the spontaneous generation of chiral shift, which induces further correction to axial current. The correlator $G_{\sigma\sigma 5}$ and $G_{n\sigma 5}$ indicates the correction to σ and n as well. It would be interesting to find out detail about this state. We leave this for future work.

Last but not the least, the normalizable mode provides an explicit example of spiral phase in meson melting phase. It would be interesting to extend this work to mesonic phase. Such an example has been found at zero temperature in [32] based on effective field theory models. It would be interesting to study the stability of such state against finite temperature fluctuation.

Note added

When this work was near complete, we learned that Qun Wang et al was about to finish a closely related work. We thank Qun Wang for sharing with us notes of their work before publication.

Acknowledgments

We are grateful to Gao-Qing Cao, Kenji Fukushima, Xu-Guang Huang, Jinfeng Liao, Yin Jiang, Qun Wang and Yi Yin for useful discussions and correspondence. S.L. is partially supported by Junior Faculty's Fund of Sun Yat-Sen University and One Thousand Talent Program for Young Scholars. He also thanks Central China Normal University for hospitality during the workshop "QCD Phase Structure III", where part of this work was done.

A Dictionary for Euclidean Correlator

To find out correlators G_{ab}, we first obtain on-shell action from (32):

$$\begin{aligned} S^{\partial}_{\rho=\Lambda} = &-\mathcal{N}r_0^4\int d^4x\sqrt{-h}\big[\frac{1}{2}\left(\delta\theta\delta\theta'\left(1-\theta'^2h^{\rho\rho}\right)+g_{\phi\phi}\phi\phi'\right)h^{\rho\rho}+\frac{1}{2}a_ta_t'h^{tt}h^{\rho\rho}+\frac{3}{4}\delta g^{(1)}_{SS}g^{SS}\theta'\delta\theta h^{\rho\rho}\\ &-\frac{1}{2}a_t\theta'\delta\theta'h^{t\rho}h^{\rho\rho}-\frac{1}{2}a_t'\theta'\delta\theta h^{t\rho}h^{\rho\rho}+\frac{3}{4}\delta g^{(1)}_{SS}g^{SS}a_th^{t\rho}\big]\\ &+\frac{1}{2}\cos^4\theta B\left(\dot{a}_t\phi-a_t\dot{\phi}\right). \end{aligned} \tag{57}$$

The asymptotics of fields can be obtained from EOM as

$$\begin{aligned} \phi &= f_0+\frac{f_2}{\rho^2}+\frac{f_h}{\rho^2}\ln\rho+\cdots,\\ a_t &= a_0+\frac{a_2}{\rho^2}+\frac{a_h}{\rho^2}\ln\rho+\cdots,\\ \delta\theta &= \frac{t_1}{\rho}+\frac{t_3}{\rho^3}+\frac{t_h}{\rho^3}\ln\rho+\cdots, \end{aligned} \tag{58}$$

with the coefficient of logarithmic terms fixed as

$$f_h=-k^2f_0,\quad a_h=-k^2a_0,\quad t_h=-k^2t_1. \tag{59}$$

Plugging (58) into (57), we find the second line always vanishes in the limit $\Lambda\to\infty$. The first line gives the following contribution

$$\begin{aligned} S^{\partial} = &-\mathcal{N}r_0^4\big[-\frac{t_1^2\Lambda^2}{8}+\frac{1}{8}\left(6m^2t_1^2-4t_1t_3+t_1t_h-4t_1t_h\ln\Lambda\right)\\ &+\frac{1}{4}\left(2a_0a_2-a_0a_h+2a_0a_h\ln\Lambda\right)+\frac{m^2}{8}\left(-2f_0f_2+f_0f_h-2f_0f_h\ln\Lambda\right)\big]+\cdots \end{aligned} \tag{60}$$

We need the following counter terms to remove quadratic divergence in (60)

$$S^{\text{counter}}_{\rho=\Lambda} = \frac{1}{2}\mathcal{N}\sqrt{-\gamma}\delta\theta^2 = \mathcal{N}\big[\frac{t_1^2\Lambda^2}{8} + \frac{1}{4}\left(t_1 t_3 + t_1 t_h \ln\rho\right)\big] + \cdots . \tag{61}$$

The coefficient of the logarithmic terms (59) is a special case of a more general relation:

$$f_h = -\Box f_0, \quad a_h = -\Box a_0, \quad t_h = -\Box t_1. \tag{62}$$

They do not encode dynamics of the theory. The corresponding logarithmic and finite terms can be removed by the following counter terms with appropriate normalizations

$$\begin{aligned}
&\mathcal{N}\sqrt{-\gamma}\delta\theta\Box\delta\theta\ln\Lambda, \quad \mathcal{N}\sqrt{-\gamma}a_t\Box a_t\ln\Lambda, \quad \mathcal{N}\sqrt{-\gamma}\phi\Box\phi\ln\Lambda,\\
&\mathcal{N}\sqrt{-\gamma}\delta\theta\Box\delta\theta, \quad \mathcal{N}\sqrt{-\gamma}a_t\Box a_t, \quad \mathcal{N}\sqrt{-\gamma}\phi\Box\phi,
\end{aligned} \tag{63}$$

Adding all counter terms to (57) and dropping contributions like $m^2t_1^2$, which do not encode dynamics of the theory, we obtain the following renormalized on-shell action

$$S^{\text{ren}} = \mathcal{N}r_0^4\left(-\frac{t_1t_3}{4} + \frac{a_0a_2}{2} - \frac{m^2f_0f_2}{4}\right). \tag{64}$$

Now we can do variation of (64) with respect to sources to obtain vev of the corresponding operators. Note that partial derivatives hit twice in each terms in the bracket. We obtain

$$\begin{aligned}
\delta\sigma &= \frac{\delta S^{\text{ren}}}{\delta t_1} = \mathcal{N}r_0^3(2\pi\alpha')\left(-\frac{t_3}{2}\right),\\
\delta n &= \frac{\delta S^{\text{ren}}}{\delta a_0} = \mathcal{N}r_0^3(2\pi\alpha')a_2,\\
\sigma_5 &= \frac{\delta S^{\text{ren}}}{\delta f_0} = \mathcal{N}r_0^4\left(-\frac{m^2f_2}{2}\right),
\end{aligned} \tag{65}$$

We use the δ symbol to indicate that the vev is on top of a nonvanishing background. Taking the derivatives once more, we obtain correlators shown in (35).

References

[1] Dmitri E. Kharzeev, Larry D. McLerran, and Harmen J. Warringa. The Effects of topological charge change in heavy ion collisions: 'Event by event P and CP violation'. *Nucl.Phys.*, A803:227–253, 2008.

[2] Kenji Fukushima, Dmitri E. Kharzeev, and Harmen J. Warringa. The chiral magnetic effect. *Phys. Rev. D*, 78:074033, 2008.

[3] D. Kharzeev and A. Zhitnitsky. Charge separation induced by P-odd bubbles in QCD matter. *Nucl.Phys.*, A797:67–79, 2007.

[4] Max A. Metlitski and Ariel R. Zhitnitsky. Anomalous axion interactions and topological currents in dense matter. *Phys.Rev.*, D72:045011, 2005.

[5] D.T. Son and Ariel R. Zhitnitsky. Quantum anomalies in dense matter. *Phys.Rev.*, D70:074018, 2004.

[6] Dmitri E. Kharzeev and Ho-Ung Yee. Chiral Magnetic Wave. *Phys.Rev.*, D83:085007, 2011.

[7] Yannis Burnier, Dmitri E. Kharzeev, Jinfeng Liao, and Ho-Ung Yee. Chiral magnetic wave at finite baryon density and the electric quadrupole moment of quark-gluon plasma in heavy ion collisions. *Phys. Rev. Lett.*, 107:052303, 2011.

[8] Gang Wang. Search for Chiral Magnetic Effects in High-Energy Nuclear Collisions. *Nucl. Phys.*, A904-905:248c–255c, 2013.

[9] L. Adamczyk et al. Beam-energy dependence of charge separation along the magnetic field in Au+Au collisions at RHIC. *Phys.Rev.Lett.*, 113:052302, 2014.

[10] Betty Abelev et al. Charge separation relative to the reaction plane in Pb-Pb collisions at $\sqrt{s_{NN}} = 2.76$ TeV. *Phys.Rev.Lett.*, 110(1):012301, 2013.

[11] Hongwei Ke. Charge asymmetry dependency of π^+/π^- elliptic flow in Au + Au collisions at $\sqrt{s_{NN}} = 200$ GeV. *J. Phys. Conf. Ser.*, 389:012035, 2012.

[12] Qi-Ye Shou. Charge asymmetry dependency of π/K anisotropic flow in U+U $\sqrt{s_{NN}} =$ 193 GeV and Au+Au $\sqrt{s_{NN}} = 200$ GeV collisions at STAR. *J. Phys. Conf. Ser.*, 509:012033, 2014.

[13] D. E. Kharzeev, J. Liao, S. A. Voloshin, and G. Wang. Chiral magnetic and vortical effects in high-energy nuclear collisions—A status report. *Prog. Part. Nucl. Phys.*, 88:1–28, 2016.

[14] Jinfeng Liao. Anomalous transport effects and possible environmental symmetry 'violation' in heavy-ion collisions. *Pramana*, 84(5):901–926, 2015.

[15] Xu-Guang Huang. Electromagnetic fields and anomalous transports in heavy-ion collisions — A pedagogical review. *Rept. Prog. Phys.*, 79(7):076302, 2016.

[16] Ioannis Iatrakis, Shu Lin, and Yi Yin. The anomalous transport of axial charge: topological vs non-topological fluctuations. *JHEP*, 09:030, 2015.

[17] Yan Wu, Defu Hou, and Hai-cang Ren. The Subtleties of the Wigner Function Formulation of the Chiral Magnetic Effect. 2016.

[18] E. V. Gorbar, V. A. Miransky, I. A. Shovkovy, and Xinyang Wang. Radiative corrections to chiral separation effect in QED. *Phys. Rev.*, D88(2):025025, 2013.

[19] Jiunn-Wei Chen, Jin-yi Pang, Shi Pu, and Qun Wang. Kinetic equations for massive Dirac fermions in electromagnetic field with non-Abelian Berry phase. *Phys. Rev.*, D89(9):094003, 2014.

[20] D. V. Deryagin, Dmitri Yu. Grigoriev, and V. A. Rubakov. Standing wave ground state in high density, zero temperature QCD at large N(c). *Int. J. Mod. Phys.*, A7:659–681, 1992.

[21] E. Shuster and D. T. Son. On finite density QCD at large N(c). *Nucl. Phys.*, B573:434–446, 2000.

[22] Shin Nakamura, Hirosi Ooguri, and Chang-Soon Park. Gravity Dual of Spatially Modulated Phase. *Phys. Rev.*, D81:044018, 2010.

[23] Hirosi Ooguri and Chang-Soon Park. Holographic End-Point of Spatially Modulated Phase Transition. *Phys. Rev.*, D82:126001, 2010.

[24] Hirosi Ooguri and Chang-Soon Park. Spatially Modulated Phase in Holographic Quark-Gluon Plasma. *Phys. Rev. Lett.*, 106:061601, 2011.

[25] Toru Kojo, Yoshimasa Hidaka, Larry McLerran, and Robert D. Pisarski. Quarkyonic Chiral Spirals. *Nucl. Phys.*, A843:37–58, 2010.

[26] Toru Kojo, Yoshimasa Hidaka, Kenji Fukushima, Larry D. McLerran, and Robert D. Pisarski. Interweaving Chiral Spirals. *Nucl. Phys.*, A875:94–138, 2012.

[27] Jan de Boer, Borun D. Chowdhury, Michal P. Heller, and Jakub Jankowski. Towards a holographic realization of the Quarkyonic phase. *Phys. Rev.*, D87(6):066009, 2013.

[28] Gokce Basar, Gerald V. Dunne, and Dmitri E. Kharzeev. Chiral Magnetic Spiral. *Phys. Rev. Lett.*, 104:232301, 2010.

[29] Keun-Young Kim, Bindusar Sahoo, and Ho-Ung Yee. Holographic chiral magnetic spiral. *JHEP*, 10:005, 2010.

[30] Martin Ammon, Julian Leiber, and Rodrigo P. Macedo. Phase diagram of 4D field theories with chiral anomaly from holography. *JHEP*, 03:164, 2016.

[31] Dmitri E. Kharzeev and Ho-Ung Yee. Chiral helix in AdS/CFT with flavor. *Phys. Rev.*, D84:125011, 2011.

[32] Tomas Brauner and Naoki Yamamoto. Chiral Soliton Lattice and Charged Pion Condensation in Strong Magnetic Fields. 2016.

[33] E. V. Gorbar, V. A. Miransky, and I. A. Shovkovy. Normal ground state of dense relativistic matter in a magnetic field. *Phys. Rev.*, D83:085003, 2011.

[34] David Mateos, Robert C. Myers, and Rowan M. Thomson. Holographic phase transitions with fundamental matter. *Phys. Rev. Lett.*, 97:091601, 2006.

[35] David Mateos, Shunji Matsuura, Robert C. Myers, and Rowan M. Thomson. Holographic phase transitions at finite chemical potential. *JHEP*, 11:085, 2007.

[36] Shinpei Kobayashi, David Mateos, Shunji Matsuura, Robert C. Myers, and Rowan M. Thomson. Holographic phase transitions at finite baryon density. *JHEP*, 02:016, 2007.

[37] Veselin G. Filev, Clifford V. Johnson, R. C. Rashkov, and K. S. Viswanathan. Flavoured large N gauge theory in an external magnetic field. *JHEP*, 10:019, 2007.

[38] Johanna Erdmenger, Rene Meyer, and Jonathan P. Shock. AdS/CFT with flavour in electric and magnetic Kalb-Ramond fields. *JHEP*, 12:091, 2007.

[39] Nick Evans, Astrid Gebauer, Keun-Young Kim, and Maria Magou. Holographic Description of the Phase Diagram of a Chiral Symmetry Breaking Gauge Theory. *JHEP*, 03:132, 2010.

[40] Carlos Hoyos-Badajoz, Karl Landsteiner, and Sergio Montero. Holographic meson melting. *JHEP*, 04:031, 2007.

[41] Carlos Hoyos, Tatsuma Nishioka, and Andy O'Bannon. A Chiral Magnetic Effect from AdS/CFT with Flavor. *JHEP*, 1110:084, 2011.

[42] Andreas Karch, Andy O'Bannon, and Ethan Thompson. The Stress-Energy Tensor of Flavor Fields from AdS/CFT. *JHEP*, 04:021, 2009.

[43] Er-dong Guo and Shu Lin. Quark mass effect on axial charge dynamics. *Phys. Rev.*, D93(10):105001, 2016.

[44] Ioannis Iatrakis, Shu Lin, and Yi Yin. Axial current generation by P-odd domains in QCD matter. *Phys. Rev. Lett.*, 114(25):252301, 2015.